JOURNAL OF GEOPHYSICAL RESEARCH, VOL. 100, NO. C10, PAGES 20,715–20,727, OCTOBER 15, 1995

Observations of wind waves in the Gulf Stream frontal zone

V. N. Kudryavtsev, S. A. Grodsky, V. A. Dulov, and A. N. Bol'shakov

Marine Hydrophysical Institute, Ukrainian Academy of Science, Sevastopol, Ukraine

Abstract. Experimental results of a study of wind waves in the Gulf Stream frontal zone are presented. Measurements of two-dimensional radar spectra of surface waves and surface current were performed during ship crossings of the Gulf Stream under different wind conditions. Waves reflected from the Gulf Stream were observed on the windward side for an along current wind. These effects resulted in a widening of the spectrum angular distribution and a deviation of the mean wave direction from that of the wind. Trapped waves were observed under against current winds. Depending on wave age, the trapped waves were either locally generated (developing waves) or entered into the jet downstream (nearly fully developed waves). Trapped waves significantly increased the wave energy locally. The experimental data are interpreted in terms of wave kinematics and the equation of spectrum evolution in the relaxation approximation.

Introduction

Interaction between surface waves and mesoscale currents of the Gulf Stream type (with length scales of 10-100 km) may be the cause of considerable spatial variability of wave parameters. The most pronounced effects, such as wave reflection by a current and waveguidelike propagation of trapped waves, have been theoretically predicted (see *Kenyon* [1971]). Substantial increase of wave energy inside a jetlike current due to the appearance of trapped waves is considered as a danger for shipping [*Gutshabash and Lavrenov*, 1986; *Irvine*, 1987]. An experimental study of these phenomena is difficult as it requires simultaneous measurements of two-dimensional (2-D) wave spectra and detailed current data over a large oceanic area.

Spaceborne synthetic aperture radar (SAR) has made it possible to obtain data on the surface wave evolution in mesoscale currents. The wave evolution in the Gulf Stream [*Beal et al.*, 1986] and in a warm core ring [*Mapp et al.*, 1985] were observed with SAR Seasat. The trapped wave system in the Agulhas Current [*Irvine*, 1987; *Irvine and Tilley*, 1988] and wave refraction by the circumpolar current [*Barnett et al.*, 1989] were observed with SAR SIR-B. Unfortunately, these observations were not supported by synchronous current measurements. The analysis of these data was based on equations of wave packet kinematics discussed by *Whitham* [1960] and *Kenyon* [1971]. In some papers [*Sheres*, 1982; *Sheres et al.*, 1985; *Barnett et al.*, 1989], an inverse approach was used to determine the current by measuring the wave kinematics. But the problem of correspondence between the real wave evolution and predictions of a simple kinematical theory should not be assumed to be trivial. At least *Beal et al.* [1986] paid attention to their explicit discrepancy.

An adequate description of wave evolution in mesoscale currents needs to take into account the wind-wave and wave-wave interactions and dissipative processes. This has been done most completely in the third-generation wave model [*WAMDI Group*, 1988]. Such a model was used by *Holthuijsen and Tolman* [1991] for calculation of wave spectra in mesoscale currents. The appearance of trapped waves locally generated within a straight jet was one of the results of these calculations which cannot be obtained using a simple kinematical description.

The main aim of this paper is to describe the results of in situ measurements of wave evolution in the Gulf Stream. Wave, wind, and current measurements were made simultaneously. Attention is primarily given to revealing the effects of reflection and trapping of waves by currents. These very effects (if they really occur) produce the greatest wave variations in a current.

Reflection and Trapping of Waves

The effects of wave reflection and trapping by current inhomogeneities are clearest when the current is uniform in some direction. The simplest model current $\vec{U}(\vec{x})$ is the straight shear current that is uniform in the x_1 direction

$$U_1 = U(x_2) \qquad U_2 = 0 \tag{1}$$

Paper number 95JC00425.
0148-0227/95/95JC-00425$05.00

A fragment of circular current may be used to simulate a curving jet

$$U_1 = -U(r)\sin\phi \quad U_2 = U(r)\cos\phi \qquad (2)$$

where r and ϕ are polar coordinates.

The kinematics of a wave packet with wave number vector $\vec{k}(t) = (k_1(t), k_2(t))$ and position $\vec{x}(t)$ in the geometrical optics approximation is described by the equations [*Landau and Lifshitz*, 1959; *Whitham*, 1960]

$$\frac{dk_i}{dt} = -\frac{\partial\Omega}{\partial x_i} \qquad c_i = \frac{dx_i}{dt} = \frac{\partial\Omega}{\partial k_i} \qquad i = 1,2 \quad (3)$$

here $\vec{c}$ is the group velocity vector, $\Omega = \omega(k) + \vec{U}\vec{k}$, $\omega = (gk)^{\frac{1}{2}}$ is the wave frequency in deep water in the absence of currents, $k = |\vec{k}|$, and g is acceleration of gravity. Solutions of (3) for the current models (1,2) were discussed in a number of papers [*Kenyon*, 1971; *Dobson and Irvine*, 1983; *Irvine*, 1987]; the general solution of (3) in quadrature for the model (2) was given by *Dulov et al.* [1986]. System (3) is Hamiltonian; hence it has integrals of motion under conditions of symmetry (in direct analogy with mechanics). For stationary current the "energy" is conserved:

$$\Omega = \text{const} \qquad (4)$$

For the current models (2) and (3), the "momentum" or the "angular momentum" is conserved, respectively:

$$p = k\cos\alpha = \text{const} \quad (\text{for (1)})$$
$$p = kr\cos\alpha = \text{const} \quad (\text{for (2)}) \qquad (5)$$

where α is the angle between the vectors $\vec{k}$ and $\vec{U}$. It can be deduced from (4) and (5) that

$$k = \frac{(\Omega - pU(x_2))^2}{g} \qquad k = \frac{(\Omega - pU(r)/r)^2}{g} \qquad (6)$$

$$\cos\alpha = \frac{gp}{(\Omega - pU(x_2))^2} \qquad \cos\alpha = \frac{gp}{r(\Omega - pU(r)/r)^2} \qquad (7)$$

where the first column corresponds to model (1) and the second one corresponds to model (2). It follows from (7) that spatial domains where $|\cos\alpha| > 1$ may exist for specified values of Ω and p. The wave packet cannot penetrate into these areas. Their boundaries $\vec{x}_b$ are given by the equation

$$|\cos\alpha(\vec{x}_b)| = 1 \qquad (8)$$

At the boundary $\vec{x}_b$, wave packet reflection takes place; that is, the group velocity component normal to the boundary changes sign. We assume for definiteness that $U > 0$. As the sign of $\cos\alpha$ is conserved (see (5)), it is convenient to separate possible situations into the case of along current wave propagation ($\cos\alpha > 0$) and opposite-to-current wave propagation ($\cos\alpha < 0$).

If the waves impinge on a straight current jet, reflection is possible for waves running with the current, and it is impossible for waves running against the current. If the current is infinite in the x_1 direction, at any point where a reflected wave exists there is also an incident wave. If the wave number vector of the incident wave is (k_1, k_2), then according to Snell's law the wave number vector of the reflected wave is $(k_1, -k_2)$.

If a uniform wave field impinges on a circular current jet, the reflection is possible for both along current propagation (see Figure 1, ray A) and contrary current propagation (ray B). As the current is nonuniform in the x_1 direction, an interpretation of this case in terms of Snell's law loses its simplicity (Figure 1). There might exist regions with two wave systems like in the straight current (Figure 1, rays A and C), only one of which (ray A) has a reflection, while the other (ray C) crosses the current without reflection.

If a wave packet runs inside a straight current, then total internal reflection in which the waves cannot leave the current is possible. Trapped waves reflect at the waveguide boundaries $\vec{x}_{b1}$, $\vec{x}_{b2}$. According to (7) and (8), the current speeds at the boundaries are equal:

$$U(x_{b1}) = U(x_{b2}) \qquad (9)$$

A similar waveguide may occur in a circular current (ray D, Figure 1), but then equation (9) is not satisfied. Thus such a waveguide is shifted relative to the current core compared with that in a straight current.

For any point x_1, the regions of the parameters (Ω,p) corresponding to any discussed situation relate one-to-one to the regions in the $\vec{k}$ plane through (4-7). Thus any wave vector $\vec{k}$ (for example, the vector corresponding to the peak of the observed wave spectrum) can be referred to one of the wave classes considered above. *Holthuijsen and Tolman* [1991] used this scheme in the $\vec{k}$ plane for interpretation of results of the model calculations of wave evolution on a straight current.

Even if a current looks almost straight (the radius of curvature is 10^3-10^4 km), the ray pattern may still reveal features characteristic of circular current [*Irvine*, 1987]. Thus proceeding from the simplified kinematical wave description (3) and the simple model of circular current (2), one should expect a real wave pattern to be very complicated if wave reflection or trapping occurs.

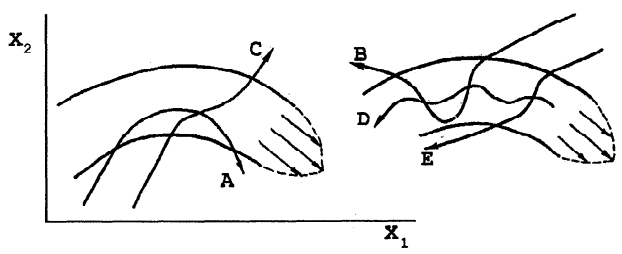

Figure 1. Ray pattern for various types of waves on a circular current: transmitted (C, E), reflected (A, B), and trapped (D) waves.

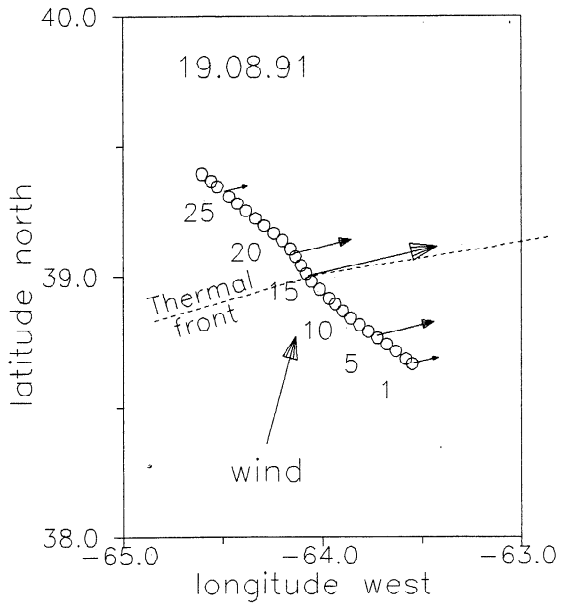

Figure 2. Scheme of experiment 6. Figure shows the spatial locations and numbering of radar images, the Gulf Stream thermal front, current direction, and mean wind direction.

Moreover, for a real current (with no symmetry features) the concepts of reflection or trapping themselves may turn out to be unconventional.

Description of the Experiment

Observations of wind waves in the Gulf Stream were carried out in August-September 1991 on board the R/V *Akademik Vernadsky* of the Marine Hydrophysical Institute (Ukrainian National Academy of Sciences). The Gulf Stream frontal zone was located using the sea surface temperature field received from the National Oceanic Atmospheric Administration satellite by ship receiving station. The measurements were performed as the ship crossed the Gulf Stream. The following parameters were measured in real time: two dimensional (2-D) radar spectra of the surface waves; mean square of ship vertical displacement; whitecap coverage; the component of surface current velocity perpendicular to the ship's track; sea surface temperature; wind velocity and air temperature. Methods of data recording and processing are given in the Appendix.

Results of wave observations for the three crossings of the Gulf Stream during strong winds (W >10 m/s) are presented below. Maps of the experiments indicating location of the thermal front and the ship track are shown in Figures 2, 6, and 10. Table 1 presents the time, mean wind velocity, and wave age for each experiment. Experiment 6 was carried out during an along current wind. In this case wave reflection is possible. Experiments 13 and 19 were carried out with a counter-current wind, when the existence of trapped waves may be expected. These experiments were performed for developing (13) and nearly fully developed (19) wind waves.

Along Current Wind

Experiment 6 was held under strong wind from the southwest. Figure 2 presents the location of the Gulf Stream thermal front and position of points where radar observations were performed. The arrows in Figure 2 show schematically the current and wind velocity vectors. Water and air temperatures, wind speed and direction, and surface current speed are shown in Figure 5.

For the observed wind direction relative to the Gulf Stream (Figure 2), one may expect wave reflection at the current's southern side. Figure 3 presents a selection of 2-D radar spectra to illustrate the main observed features of cross-current variability. The vertical axis in Figure 3 is directed to the north, the horizontal one to the east. Spectra numbering corresponds to the numbers of radar images in Figure 3. The 180° uncertainty in wave direction has been eliminated from radar spectra using visual observations.

The main characteristic of the data obtained is the apparent decrease of the spectrum angular width from the windward (southern) side of the current (the lower part of Figure 3) to the leeward (northern) side. One can distinguish two local maxima A and B in radar spectra. On the Gulf Stream northern (downwave) side the radar spectra have in general a one-peak structure (system A; see point 21 in Figure 3). The direction of peak wave number vector is close to that of the wind. On the Gulf Stream southern (upwave) side, the radar spectra have a wider angular distribution. In these spectra one may distinguish the local maximum corresponding to the wind direction (system A) and another local maximum in which the wave number vector deviates clockwise from the wind direction (system B).

Table 1. Data Summary

Case	Date (1991)	Mean Wind Speed m/s	Wave Age $\omega_p W/g$	Mean Wind Direction (to), deg	Current Direction deg	Radius of Current Curvature, km
6	Aug. 19	14	1.14	15	75	600
13	Aug. 25	15	1.46	220	70	390
19	Sept. 2	14	0.93	200	55	220

Direction is clockwise from the north.

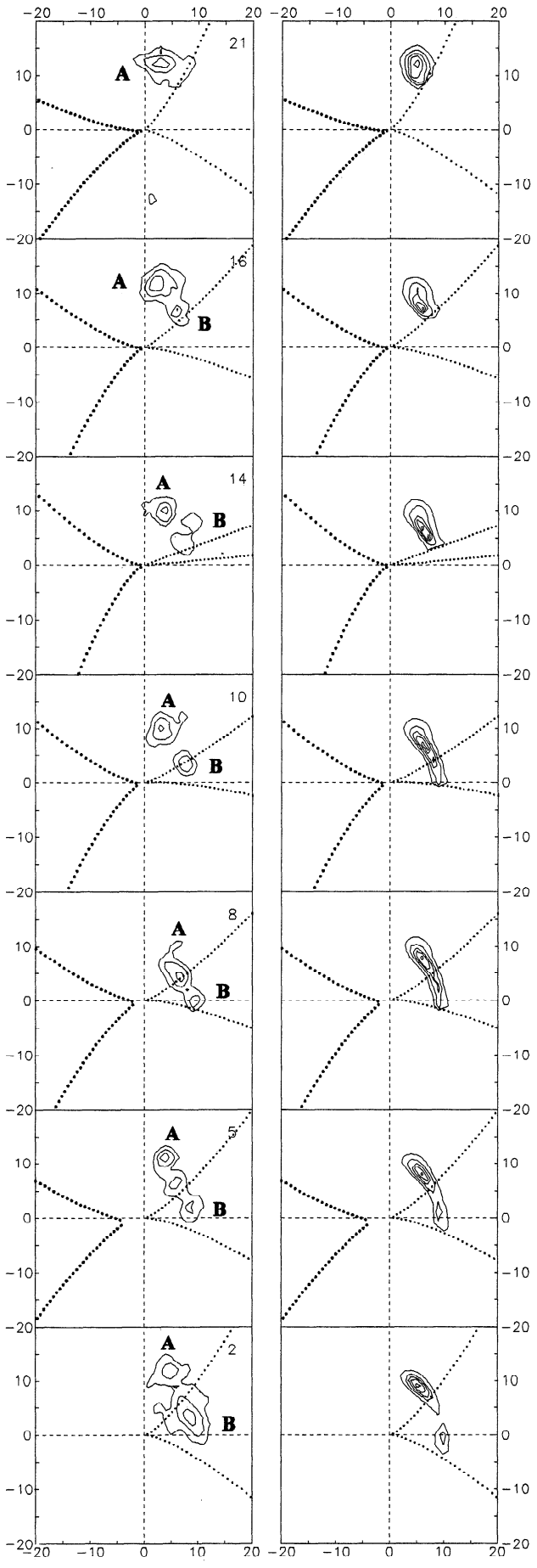

In order to interpret these spectra in the frame of kinematic theory (equations (6) and (7)), the curvature of the front in the experimental region (Figure 2) was approximated by a circle. Its radius and the direction of the tangent at the point of the front where the ship crossed are presented in the Table 1 as radius of curvature and current direction. Radial profiles of current speed are taken from the measurements (Figure 5a). The directional sectors in which waves can be trapped (dark symbols) and reflected (light symbols) are indicated in Figure 3. The symmetry axis of these sectors parallels the current direction. The sector of reflected waves at the southern slope (spectra 2-10) corresponds to wave packets that could not penetrate into the northern part of the current. The similar sector on the northern slope (spectra 14-21) corresponds to wave packets that due to reflections could not penetrate into the southern part of the Gulf Stream. This sector, as well as the sector of trapped waves, is forbidden for waves falling on the current from the south.

Local maximum A is outside of all sectors and thus could be referred to as the waves simply crossing the Gulf Stream (transmitted waves). At the southern current slope the local maximum B is within the sector of reflected waves, and thus it can represent waves reflected by Gulf Stream (spectra 2-10). One can see from Figure 3 the absence of wave energy in the forbidden sectors. For a straight current, two wave systems should be observed in the sector of reflected waves, that is, incident and reflected ones with wave number vectors being symmetrical with respect to the current direction. The fact that this relation is not satisfied in analyzed spectra may be due to jet curvature.

Obviously, the model of circular current is good for a description of the real current in only a small region. If the scale of wave generation exceeds greatly the scale of this local region a consideration of the actual current field may be important for the wave kinematics analysis. Figure 4 illustrates the current field reconstructed using the measured current profile (Figure 5a) and thermal front configuration. It was assumed that in any section normal to the temperature front the velocity profile corresponds to the measured one and the current direction coincides with that of the front. Figure 4a shows the wave rays corresponding to the local spectral maxima A (light dots) and B (dark dots). The rays are calculated using (3). The range of wind direction variation during the experiment is shown by two vectors. The rays of

Figure 3. Selection of radar spectra observed in experiment 6 (left column) and model wave elevation spectra (right column). Discretization in wave number is $\Delta k_x = \Delta k_y = 5.45 \times 10^{-3}$ rad/m. Spectrum isolines are drawn in $0.2S_{\max}$ up to $0.9S_{\max}$ ($S_{\max}$ is spectrum maximum level). The spectral numbering corresponds to that of Figure 2. Calculated sectors of reflected and trapped waves are shown with light and dark symbols, respectively. Different wave systems are marked with different letters.

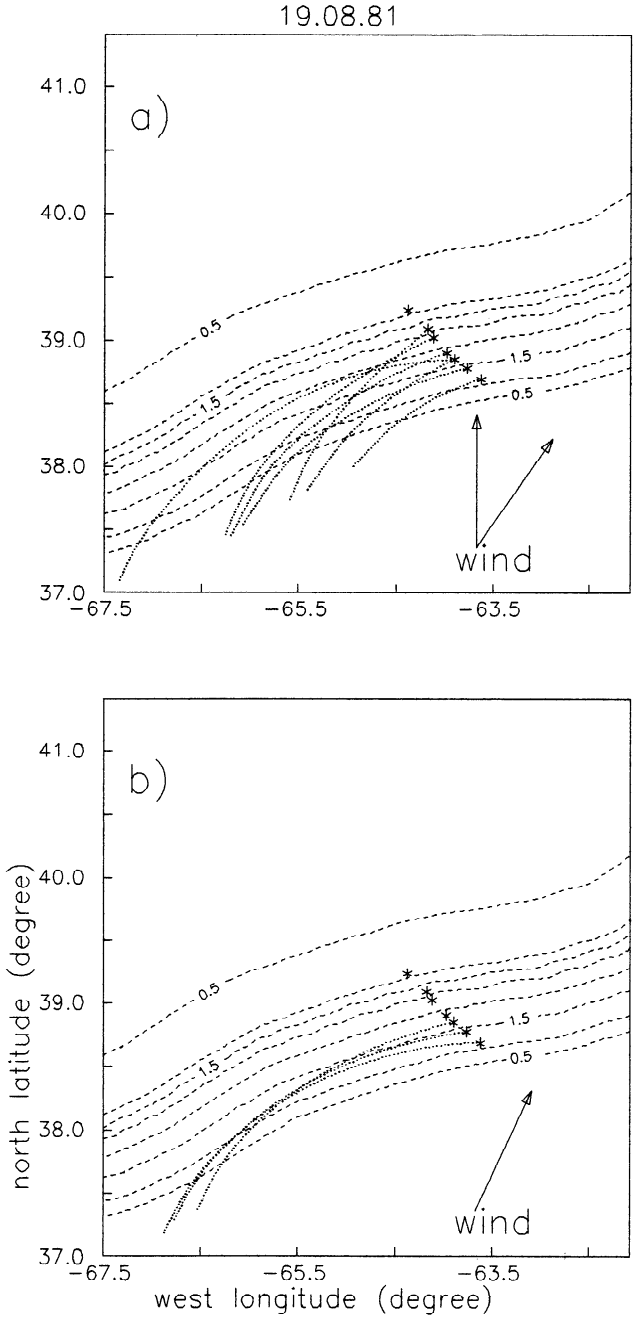

Figure 4. Reconstructed surface current modulus field. The digits mark speed isolines in meters/second. The wave rays calculated for local spectral maxima A and B of the (a) observed radar spectra and (b) calculated spectra (see Figure 3) are shown with light and dark symbols, respectively. The arrows show variability of (a) wind direction and (b) mean wind direction. The wind vector length equals 1/4 of background wave fetch.

system A cross the current. The rays of system B enter the current further west than the rays of system A (see Figure 4a). Thus the local angle of incidence relative to the normal of the current is greater for system B than for system A due to jet curvature. It critically affects the ray pattern. As a result, some waves of system B propagate along the rays which cannot penetrate to the northern slope of the Gulf Stream.

Consider the observed spectra in terms of a simple model of the wind wave spectrum evolution on the current in the relaxation approximation [*Alpers and Hasselmann*, 1978]. The more complete model based on the third-generation wave model [*WAMDI Group*, 1988] was realized by *Holthuijsen and Tolman* [1991]. However, an application of such a model is beyond the scope of this paper. We assume the governing equation in the form

$$\frac{dN}{dt} = -\frac{\Delta N}{\tau} \tag{10}$$

where N is spectrum of wave action, $\Delta N = N - N_0$, τ is the parameter of spectrum relaxation, and N_0 is the unperturbed spectrum which is stationary and hor-

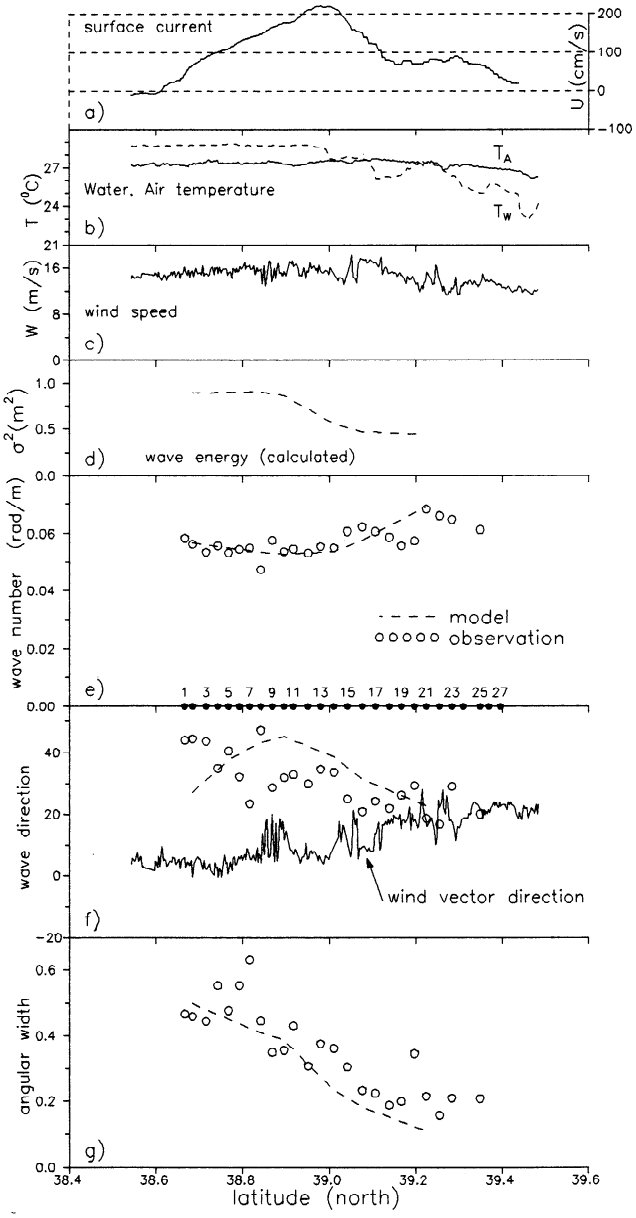

Figure 5. Variability of hydrometeorological parameters and integral parameters of wave spectra along the ship route. The solid circles and appropriate numbers show the position and numbering of radar images.

izontally uniform. Equation (10) describes variations of wave action spectrum along characteristics $\vec{k}(t)$ and $\vec{x}(t)$ which are solutions of (3).

As is known, the dynamics of spectral peak of nearly fully developed waves is governed by wave-wave interactions, and thus it cannot be described by (10) being local in $\vec{k}$ plane. Nevertheless, we shall consider this equation as a reasonable approximation, modeling the ability of waves to relax to the unperturbed state after cessation of action of the perturbing sources.

We analyze the waves of spectral peak (only these waves are observed by radar). Therefore we assume that τ for these waves may be defined through dimensionless fetch x

$$\tau = \frac{Wx}{g} \tag{11}$$

where $x = Xg/W^2$, and X is a wave fetch. Dimensionless fetch is determined here via the spectrum peak frequency $\omega_p = 2\pi f_p$ using the empirical dependence of *Donelan et al.* [1985]

$$\frac{W\omega_p}{g} = 11.6x^{-0.23} \tag{12}$$

The background spectrum is defined as a 2-D Gaussian function with wave number and angular width equal to $0.1k_p$ and 10°, respectively. The wave number vector of the model spectral peak is assumed to be equal to its average value for system A ($k_p = 0.065\ rad/m$, $\Theta_p = 25°$). In Figure 3 the model calculations of 2-D spectra are shown for those spatial points where radar spectra were obtained. The noticeable feature of the calculated spectra consists of the presence of reflected waves. They result in either the appearance of local spectral maximum B, lying in sectors of reflected waves (points 2-5), or the increase of the angular width of spectra (points 8-10). Note the absence of energy in forbidden sectors at points 14-21. The sharp cutoff of spectra at the boundaries of these sectors is the well-known effect of wave filtration by current [*Dreizis et al.*, 1986]. The wave rays corresponding to maxima A and B of calculated spectra are presented in Figure 4b.

Spectrum variation across the Gulf Stream may be presented by variation of its integral parameters. These parameters (average wave number, direction, and angular width), calculated using (A1), are presented in Figure 5. Calculations were performed by integration over whole spectra without separation on wave systems. The average wave number is less varied. Average wave directions at the southern slope differ sufficiently from the wind direction due to the presence of reflected wave components. The same cause produces a twofold excess in spectrum angular width at the southern current slope as compared to the northern one. The model calculations reproduce the observations well.

Contrary Current Wind

Experiment 13 was carried out in strong winds from the northeasterly direction and developing waves (Figure 6). Under these conditions the appearance of waves locally generated and then trapped by current can be expected.

In Figure 9 the surface current speed, wind speed, and air and water temperatures across the Gulf Stream as well as points of radar observations are plotted. The selection of radar spectra is presented in Figure 7. In this figure the sectors corresponding to waves trapped and reflected by the model circular current are also plotted. Outside the Gulf Stream (points 1-10) one wave system (A) is observed. These waves (falling on the current) propagate in the along wind direction. The dimensionless frequency of the spectral peak equals $W\omega_p/g = 1.46$; that is, these are developing waves. At the northern Gulf Stream slope the falling waves (system A) are refracted by current shear and the wave number vector of the spectral peak turns counterclockwise from the wind direction toward the front normal.

On the current southern slope (starting from point 13), wave system A is no longer distinguished in radar spectra in the background of a new wave system (B). The wave number and direction of this system differ from those of system A. It is noticeable that the "sudden" appearance of system B waves takes place in the same spatial point where the sector of trapped waves appeared (point 13, Figure 7). The location of the system B waves in these sectors leads to the conclusion that a trapped wave was observed.

In Figure 8 the wave rays calculated for spectral maxima of systems A and B are plotted. The current field is reconstructed with the curve of the thermal front and the measured current profile. The arrows show the wind direction, with an arrow length equal to the dimensional scale of incident wave generation (this scale is estimated from (12) for $W\omega_p/g = 1.46$). The ray pattern divides

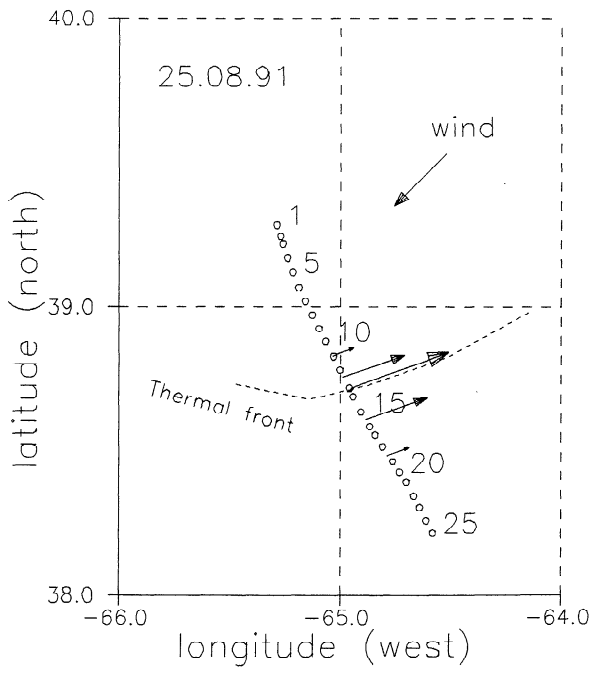

Figure 6. The same as in Figure 2. Experiment 13.

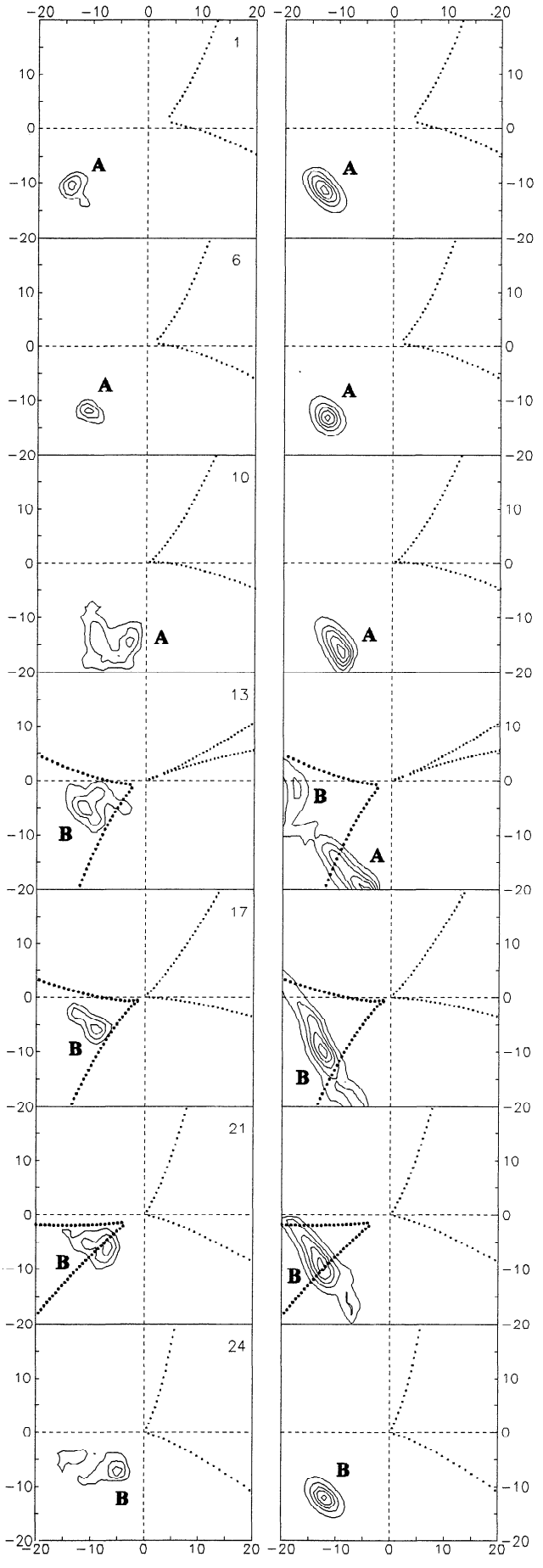

into two clusters. The waves of system A are generated northward of the Gulf Stream. Wave rays of system B oscillate inside the jet; that is, they are locally trapped. The current has complicated geometry; thus waves being locally trapped in one part of the current can leave the current in another part. Such a situation was observed for the waves of system B in spectra 21 and 24. As at a scale of their generation, the wave rays of system B are localized inside the current; these waves are locally generated within the Gulf Stream.

Compare the observational data with model calculations. In these calculations the background spectrum parameters are defined by integral parameters of the radar spectrum at point 1 (Figure 7): $k_p = 0.093$ rad/m, $\Theta_p = 225°$. Calculated 2-D wave spectra are shown in Figure 7. The incident wave system (A) and trapped wave system (B) can be identified on the model spectra. In contrast to radar observations, system A is distinguished in model spectra up to point 13 where the trapped waves "suddenly" appeared.

Wave rays corresponding to model spectra local maxima are plotted in Figure 8b. The model ray pattern is similar to that calculated for radar spectra (Figure 8a). The rays are also divided into two clusters. The wave field at the current northern slope is formed by the waves generated outside the Gulf Stream. At the southern slope the waves are trapped and locally generated within jet.

Figure 9 presents the averaged wave number $\bar{k}$ and direction $\bar{\Theta}$ of systems A and B (calculated using (A1)) for observed and model spectra. Deviation of the direction of wave system A from the wind direction and steplike changes in $\bar{k}$ and $\bar{\Theta}$ near the midstream (where one wave system replaces another) are the most vivid peculiarities of the observed data.

Variations in $\bar{\Theta}$, as mentioned above, are of clear ray interpretation. In particular, for system A they are induced by wave refraction on current. The calculated values of $\bar{\Theta}$ satisfactorily reproduce the measurements. However, sharp variation in the wave number vector induced by wave system change relates to the peculiarities in generation of the trapped waves. These peculiarities are not clear for us but were obtained in numerical experiments by *Holthuijsen and Tolman* [1991]. The simple model used here does not describe wave development; that is why the calculated wave numbers of system B are greater than the measured ones.

Figures 9d and 9e illustrate the distribution of whitecap coverage and the mean square vertical displacement of the ship σ^2. In the region of trapped waves, the sharp increase of wave energy (assumed to be related to σ^2) and whitecap coverage were recorded. These values are 2-3 times larger than their background values. This increase occurs in spite of a wind speed decrease, and thus

Figure 7. The same as in Figure 3. Experiment 13.

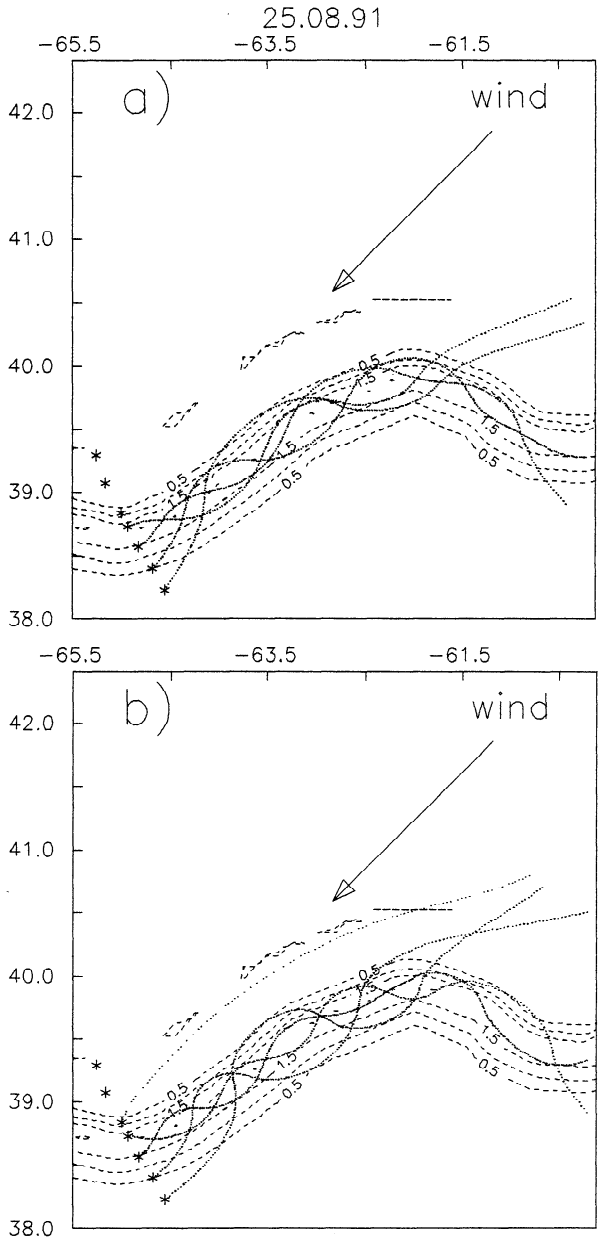

Figure 8. The same as in Figure 4. Experiment 13. Wind vector arrows show mean wind direction and have a length equal to dimensional fetch of the background waves.

may be caused by trapped waves. Model calculations of wave energy

$$\int N(\vec{k})\omega(k)d\vec{k} \qquad (13)$$

describe this increase at current southern slope (Figure 9e, dashed line).

Nearly Fully Developed Waves Under the Wind Contrary to Current

Experiment 19 was performed under strong wind contrary to the Gulf Stream. But in distinction to experiment 13, the background waves were nearly fully developed (the average dimensionless frequency during the experiment was equal to $W\omega_p/g = 0.93$). The experiment area, current speed distribution, and meteorological parameters are shown in Figures 10 and 13.

Figure 11 presents the selection of radar spectra. The spatial points where they were obtained are shown in Figures 10 and 13. On the images obtained on the current northern slope (upwave side) and outside the current (images 36-22), one can observe only one wave system (A) running approximately along wind. On the Gulf Stream southern slope (downwave side) the radar spectra contain the second wave system (B) propagating approximately opposite to current (images 20-9). This system disappears on the southern periphery of the Gulf Stream (images 8-1).

The wave number sectors corresponding to reflected and trapped waves are shown in Figure 11. These sec-

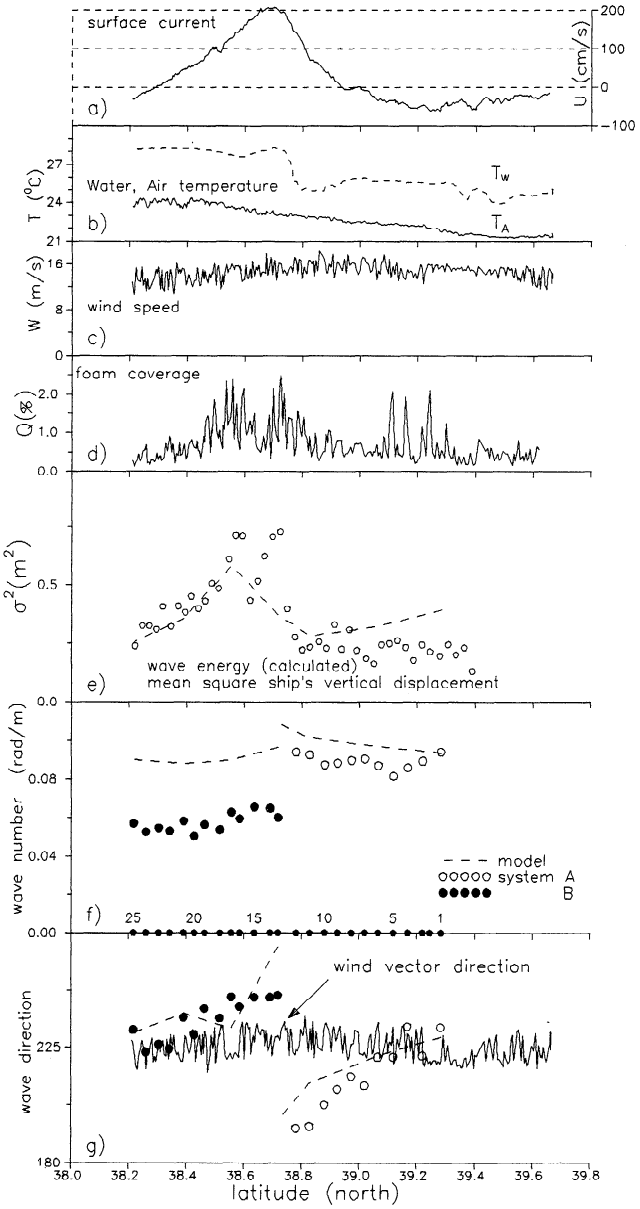

Figure 9. The same as in Figure 5. Experiment 13.

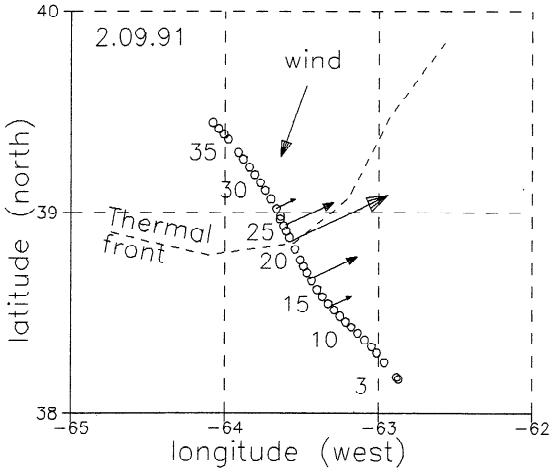

Figure 10. The same as in Figure 2. Experiment 19.

tors are calculated for the circular current that approximates the Gulf Stream meander in the vicinity of the experimental area (Figure 10). For this model of the current, the sector of trapped waves occurs only on the southern slope of the current. It should be noted that observed wave system B (as in experiment 13) appears and disappears simultaneously with the trapped wave sector. The fact that the energy of these waves is localized within this sector makes it possible to interpret wave system B as a system of waves trapped by the Gulf Stream.

Wave system A is observed in all spectra. On the northern Gulf Stream periphery these waves propagate approximately along the wind (Figure 11, point 34). Inside the Gulf Stream they refract. On the southern side of the frontal zone, wave system A does not recover its initial direction. This may be explained by the mean cyclonic vorticity causing the mean deviation of wave rays [*Kenyon*, 1971].

Figure 12a presents the wave rays related to the spectral peaks of systems A and B. They are calculated for the current field reconstructed (as previously) through the thermal front line and measured speed profile. In the vicinity of the experimental area, the Gulf Stream experiences wavelike oscillations leading to changes in mean vorticity along the current. The age of the observed waves ($W\omega_p/g = 0.93$) corresponds to a dimensional fetch of 1000 km, which exceeds the size of area considered (Figure 10). Thus the observed waves were generated outside the Gulf Stream. As in the previous case the wave rays are divided into two groups. The rays corresponding to system A are of the form typical for simple wave refraction on the contrary current. System B wave rays have a more complicated character. They penetrate into the Gulf Stream through the anticyclonic meander and, propagating along the current, undergo internal reflections. Consequently, the waves of

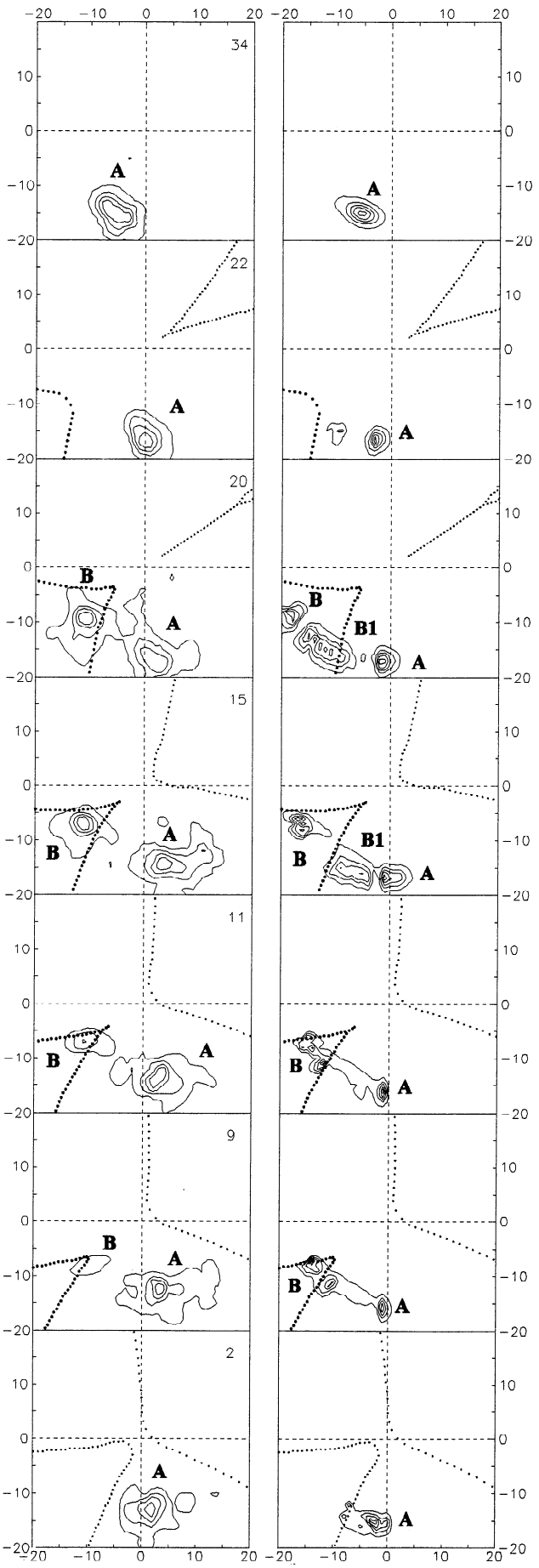

Figure 11. The same as in Figure 3. Experiment 19. Discretization in wave number is $\Delta k_x = \Delta k_y = 2.73 \times 10^{-3}$ rad/m.

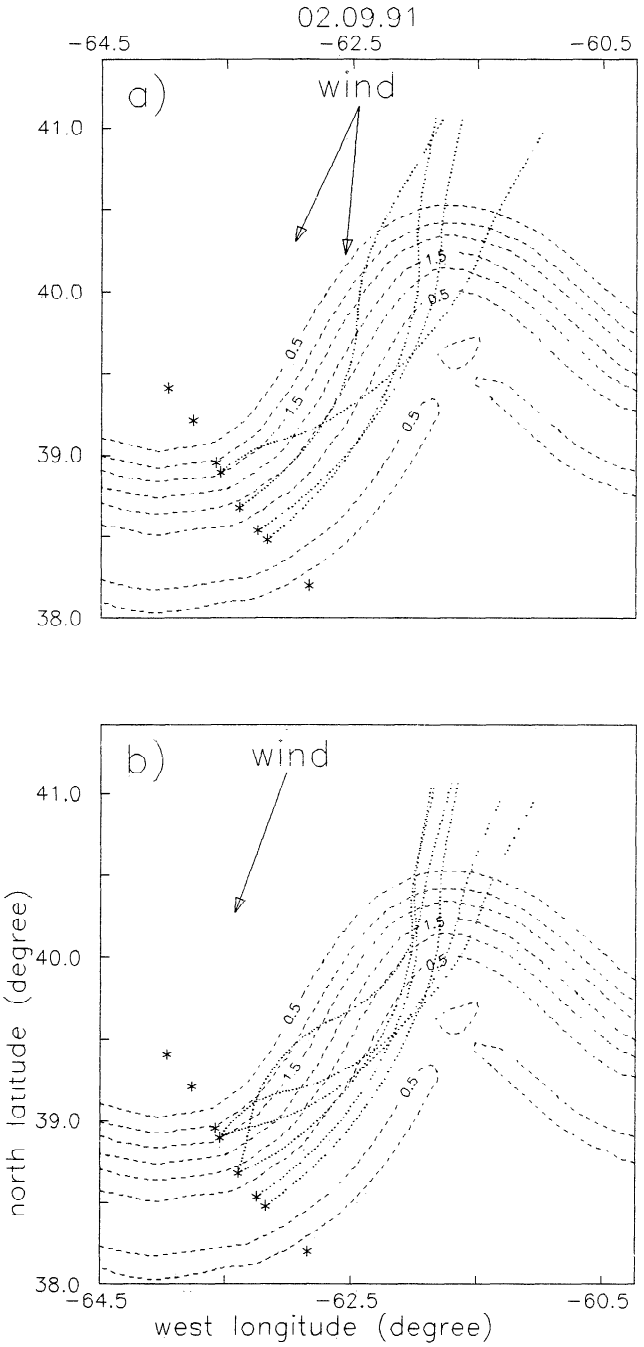

Figure 12. The same as in Figure 4. Experiment 19. Wind vector length is arbitrary. Two arrows in Figure 12a represent the observed variability in wind direction during the experiment.

system B may be interpreted as locally trapped. Note that in this case the group velocity of trapped waves is 1.5 times greater than that in experiment 13. Thus the trapped wave ray oscillation period in experiment 19 is greater than that in experiment 13 (compare Figures 8 and 12).

The model spectra are shown in Figure 11. In general, the structure of these spectra is similar to the structure of the observed radar spectra. One can distinguish local spectral maxima that can be considered as analogous to wave systems A and B on the radar spectra. Wave system B appears in the model calculations at the same points where one can observe trapped waves on the radar spectra.

Figure 12 shows wave rays related to local maxima A and B of the model spectra. There are three rays in points 20 and 15 as the third local maximum (B1) can be distinguished on the model spectra. The model wave rays are very similar to wave rays calculated for radar spectra. The model rays are also grouped into two clusters corresponding to the transmitted waves (A) and waves that are locally trapped (B). It should be emphasized that, in contrast to experiment 13 (where the observed trapped waves were generated within the Gulf Stream), the waves of system B propagate as free waves (the scale of their generation exceeds the scale of their path length inside current).

Figure 13 presents the distribution of integral parameters of observed and model wave spectra across the current. During the experiment the wind speed decreased monotonically (Figure 13c), apparently resulting in an increase in the observed wave number of system A (Figure 13f) and a decrease in the mean square ship vertical displacement σ^2 (Figure 13e). The linear trends of these parameters are shown by a solid line. The local maximum of $\bar{k}$ relative to its trend is distinguished in the vicinity of the maximum current velocity (Figure 13f). The same increase in $\bar{k}$ follows from the model calculations, but the increase is less than that observed.

Northward of the Gulf Stream the observed waves of system A propagate along wind. Inside the current they refract deviating counterclockwise from the wind direction toward the normal of the front line. In the southern part of the Gulf Stream, system A waves recover their initial direction only partially, which may be related to Gulf Stream mean cyclonic vorticity. The model calculations of system A wave direction are in reasonable agreement with observations (Figure 13h).

Figures 13g and 13h present calculated and observed wave number and direction for system B. The direction of these waves deviates from the wind direction and coincides with local orientation of the front. System B wave number vector modulus decreases across the southern current slope. This is shown in both the observational data and the calculation results. Systematic differences between model and observed values of $\bar{k}$ are likely related to wave field nonstationarity. It should be noted that there is no strong difference between the wave numbers of the trapped and transmitted waves. This means that waves of both systems propagate on a current as free waves; that is, while the wave runs inside the current, the "energy sources" (wind input, nonlinear interaction, and dissipation) do not affect the spectrum significantly.

In the region of trapped waves, the mean square of the ship vertical displacement grows to almost twice the background level given by the trend of σ^2 (Figure 13e). The whitecap coverage also increases here (Figure 13c). The observed anomalies in σ^2 and Q may be explained by the ocean surface "excitement" caused by superpo-

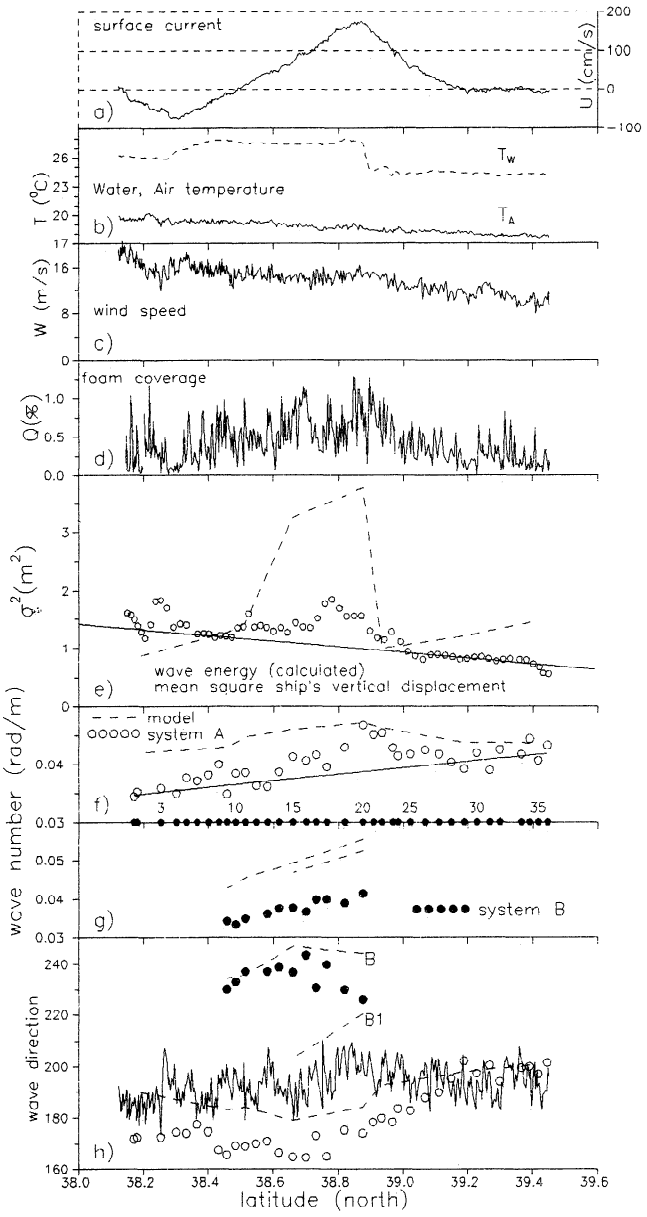

Figure 13. The same as in Figure 5. Experiment 19. Monotonic variations in mean wave number of system A and mean square ship vertical displacement are shown with straight lines. The solid line in Figure 13h shows the observed wind vector direction.

sition of wave systems A and B. In model calculations of wave energy, this effect is overestimated (Figure 13e, dashed line).

Summary

Analyses of wave kinematics on jetlike current predict the existence of waves of three types: (1) those transmitted through a current, (2) those reflected by a current, and (3) those trapped in a current [*Kenyon*, 1971]. These types of waves manifest themselves in a form of local spectral maxima in calculations of the wave field on a jet current performed by the models of various complication levels. In particular, all these types of waves have been obtained using a third-generation wave model [*Holthuijsen and Tolman*, 1991]. However, the real pattern of the wave field in a zone of strong currents is not completely clear.

Ship observations of waves in the Gulf Stream were aimed mainly at verifying the existence of the three wave types. Such a possibility was realized during the experiments performed under two meteorological situations: with the wind velocity vector having (1) along current and (2) counter-current components. In the first case the system of reflected waves was observed on the Gulf Stream windward (upwave) side. Conclusions on the presence of reflected waves were made from the analysis of wave rays related to the local maxima of the observed radar spectra. The reflection of waves appeared as a combined result of the current shear and upstream curving of the Gulf Stream. The last had increased the local angle of incidence of waves relative to the normal of current. Superposition of waves that had entered the current and were transmitting through it and waves reflected at the upstream part of the current resulted in a substantial increase of the spectrum angular width and a deviation of the wave average direction from that of the wind.

Two experiments were performed with the counter-current wind. They differed from each other by the fact that in the first experiment the background incident waves were developing (the dimensionless frequency was 1.4), whereas in the second experiment they were nearly fully developed (with dimensionless frequency of 0.98). The analysis of wave rays showed that in both cases strong variability of the measured spectra is caused by the presence of wave components locally trapped by the current. The observed variability has its own specificity determined by wave age. For developing waves the scale of generation was smaller than the wave "path length" along the current. In this case the analysis of the wave ray pattern permitted the division of the wave field into two parts: at the Gulf Stream northern slope waves were generated outside the Gulf Stream and refracting on the current; at the southern slope the observed waves were generated inside the Gulf Stream and locally trapped. In the vicinity of midstream, the replacement of wave systems was observed, accompanied by a sharp change in wave direction and decrease in wave number.

As the scale of generation of nearly fully developed waves is larger than their path length inside the current, the wave ray pattern made it possible to consider the wave field as the superposition of two wave systems. The first wave system was a transmitted one and has been observed in all points across the Gulf Stream. The second system (observed only at the southern slope) was locally trapped and entered the Gulf Stream downstream through the anticyclonic meander. A sharp change in the ocean surface state in the region where trapped waves exist resulted in an increase of the ship mean square vertical displacement and foam coverage for both cases. This result supports the hypothesis

on the origin of anomalous waves in the Agulhas Current region as waves trapped by a current [*Gutshabash and Lavrenov*, 1986; *Irvine*, 1987].

Appendix: Methods of Data Acquisition and Processing

Radar System

Two-dimensional wave spectra were estimated using radar images of the sea surface obtained with the system consisting of ship radar (HH, X band) and a computer. The radar station provides resolution of 10 m×10 m (for distance $R < 1$ km) in radial and azimuthal directions. Sea surface images were obtained by digitizing the radar video output with compensation for mean attenuation in the far field, averaging 10-15 probing pulses within an antenna turn angle of 0.4°, and recording in polar coordinates on the computer. For further processing we used the fragment of the radar image oriented upwind, which was transformed into square matrix with the dimensions of 128 × 128 points and spatial resolution $\Delta r = 10$ m or $\Delta r = 20$ m, depending on wave conditions.

Using the procedure of moving average, the fragment of the radar image was divided into "high frequency" (scales of surface waves) and averaged parts. Two-dimensional spectra were calculated from the "high-frequency" part of the field normalized by the averaged one.

The final spectrum was obtained by the averaging of four successive (in time) radar spectra with additional smoothing over squares of 3×3 in k space. It provided 72 degrees of freedom for final spectrum estimation.

It should be noted that the noise level S_{noise} resulting from the spikelike structure of radar images was present in radar spectra. Its level was estimated as $S_{\text{noise}} = nS_{\max}$, where $S_{\max}$ is spectral peak value. The value n varies within $0.2 < n < 0.5$, depending on image smoothing and wind speed. The following parameters were accepted: for experiment 19, $\Delta r = 20$ m and $n = 0.2$; for experiments 6 and 13, $\Delta r = 10$ m and $n = 0.5$.

The relation between the radar and surface wave spectra is determined by a two-dimensional modulation transfer function (MTF). The MTF is conditioned by either scattering peculiarities at low grazing angles or characteristics of the radar system. The only known estimation of the MTF for the ship radar station was obtained by the method of statistical modeling [*Ziemer and Rosental*, 1987]. It follows from these calculations that the MTF suppresses short wave components; that is, only waves of the spectral peak can be distinguished in the radar spectra.

The MTF for the radar used is unknown. Therefore we analyzed only those parameters of the radar spectra for which the variability must reflect the variability of surface wave spectra. Among these parameters we chose the following: the number of wave systems, the wave number vector of the wave system, and the angular width of radar spectra.

In order to increase the stability of the spectral peak parameter estimations, the wave number $\bar{k}$, general direction $\bar{\Theta}$, and angular width $\Delta\Theta$ were determined through the spectral moments calculated over $\vec{k}$ space, where $S > S_{\text{noise}}$ using the following relations [*Longuet-Higgins*, 1957].

$$m_{pq} = \int k_1^p \, k_2^q \, S(\vec{k}) d\vec{k}$$

$$\bar{k} = |(m_{01}/m_{00}, m_{10}/m_{00})| \qquad \bar{\Theta} = \operatorname{atan}(m_{10}/m_{01}) \tag{A1}$$

$$\Delta\Theta = \left[\frac{m_{20} + m_{02} - \left((m_{20} - m_{02})^2 + 4m_{11}\right)^{\frac{1}{2}}}{m_{20} + m_{02} + \left((m_{20} - m_{02})^2 + 4m_{11}\right)^{\frac{1}{2}}} \right]^{\frac{1}{2}}$$

For spectra with more than one local maxima, these calculations were performed for each wave system. The separation of wave systems in k plane was done manually.

Near Surface Current Velocity

The near surface current velocity was measured by geomagnetic electrokinetograph. The instrument measures the electromotive force induced in a cable towed by the ship and moving with the ship through the Earth's magnetic field [*Von Arx*, 1950]. Spacing between electrodes was 100 m. The current velocity component normal to the instrument was continuously recorded. The accuracy of speed estimation was 10 cm/s.

Wave Breaking

The percentage of whitecap coverage was measured with an optical photometer. The device footprint was oriented approximately normal to the ship course outside the Sun's glitter pattern. The initial data representing breaking events were averaged over an area of about 300 × 650 m with an averaging time of 100 s.

Mean Square of Ship Vertical Displacement

Mean square of the ship vertical displacement σ^2 was calculated from the data of an accelerometer installed on board the ship. The accelerometer registered the ship vertical acceleration with time discreteness of 0.25 s. The current value of σ^2 was determined through the current frequency spectrum of vertical accelerations $S_a(\omega)$ as $\sigma^2 = \int \omega^{-4} S_a(\omega) d\omega$. We assume that the increase in σ^2 is related to the increase in the wave energy.

Meteorological Parameters and Water Temperature

The apparent wind velocity was measured by a vane sensor with accuracy of 0.3 m/s and 1° in speed and direction, respectively. The actual wind velocity was calculated using the ship velocity. Air temperature was

measured by a copper thermometer located inside a well-ventilated reservoir protected from the solar radiation, with absolute accuracy 0.5°C. The meteorological sensors were installed at the height of 21 m. The ocean surface temperature was determined with towed thermistor with an accuracy 0.1°C.

Acknowledgments. We would like to thank Gennady Korotaev (MHI) for assistance in the organization of the experiment described in this publication, and Alexander Babanin (MHI) for allowing use of his accelerometer data. The analysis of experimental data was made possible in part by grant UD9000 from the International Science Foundation.

References

Alpers, W., and K. Hasselmann, The two-frequency microwave technique for measuring ocean wave spectra from the airplane or satellite, *Boundary Layer Meteorol., 13*, 215-230, 1978.

Barnett, T. P., F. Kelley, and B. Holt, Estimation of the two-dimensional ocean current shear field with a synthetic aperture radar, *J. Geophys. Res., 94*(C11), 16,087-16,095, 1989.

Beal, R. C., T. W. Gerling, D. E. Irvine F. M. Manaldo, and D. G. Tilley, Spatial variations of ocean wave directional spectra from the Seasat synthetic aperture radar, *J. Geophys. Res., 91*(C2), 2433-2449, 1986.

Dobson, E. B., and D. E. Irvine, Investigation of Gulf Stream ring detection with space borne altimeter using mean sea height, wave height and radar cross section, Rep. JHU/APL SIR3U-005, 51 pp., Space Dep., Appl. Phys. Lab., Johns Hopkins Univ., Laurel, Md., 1983.

Donelan, M. A., J. Hamilton, and W. H. Hui, Directional spectra of wind-generated waves, *Philos. Trans. R. Soc. London, A, 315*, 509-562, 1985.

Dreizis, Y. I., I. G. Katarzhi, and E. N. Pelinovsky, Filtration of waves by shear current (in Russian), *Vodn. Resurn., 1*, 105-109, 1986.

Dulov, V. A., V. N. Kudryavtsev, and V. V. Malinovsky, An eddy manifestation in wind wave field (in Russian), *Morsk. Hydrofizicheskii Zurnal, 2*, 44-52, 1986.

Gutshabash, Y. S., and I. V. Lavrenov, Swell transformation in the Cape Agulhas Current, *Izv. Acad. Sci. USSR Atmos. Oceanic Phys.*, Engl. Transl., *22*(6), 494-497, 1986.

WAMDI Group, The WAM model–a third generation ocean wave prediction model, *J. Phys. Oceanogr., 18*(12), 1775-1810, 1988.

Holthuijsen, L. H., and H. L. Tolman, Effects of the Gulf Stream on ocean waves, *J. Geophys. Res., 96*(C7), 12,755-12,771, 1991.

Irvine, D. E., Extreme waves in the Agulhas: A case study of wave-current interactions, *Johns Hopkins APL Tech. Dig., 8*(1), 100-106, 1987.

Irvine, D. E., and D. G. Tilley, Ocean wave directional spectra and wave-current interaction from shuttle imaging radar-B synthetic aperture radar, *J. Geophys. Res., 93*(C12), 15,389-15,401, 1988.

Kenyon, K. E., Wave refraction in ocean currents, *Deep-Sea Res., 18*, 1023-1034, 1971.

Landau, L. D., and E. M. Lifshitz, *Fluid Mechanics*, 536 pp., Addison-Wesley, Reading, Mass. 1959.

Longuet-Higgins, M. S., Statistical analysis of random moving surface, *Philos. Trans. R. Soc. London, 249*(966), 321-360, 1957.

Mapp, G. R., C. S. Welsh, and J. C. Munday, Wave refraction by warm core rings, *J. Geophys. Res., 90*(C4), 7153-7162, 1985.

Sheres, D., Remote synoptic surface current measurements by gravity waves: A method and its test in a small body of water, *J. Phys. Oceanogr., 12*, 200-207, 1982.

Sheres, D., K. E. Kenyon, R. L. Bernstein, and R. C. Beardsley, Large horizontal surface velocity shears in the ocean obtained from images of refracting swell and in situ moored current data, *J. Geophys. Res., 90*(C3), 4943-4950, 1985.

Von Arx, W. S., An electromagnetic method for measuring the velocities of ocean currents from a ship under way, *Pap. Phys. Oceanogr. Meteorol., 11*(3), 1-62, 1950.

Whitham, G. B., A note on group velocity, *J. Fluid Mech., 9*, 347-352, 1960.

Ziemer, F., and W. Rosental, On the transfer function of a shipborne radar for imaging ocean waves, in *Proceedings of IGARSS '87, vol. 2*, pp. 1559-1564, University of Michigan, 18-21 May, 1987.

A. N. Bol'shakov, V. A. Dulov, S. A. Grodsky, and V. N. Kudryavtsev, Marine Hydrophysical Institute, Ukrainian Academy of Science, Kapitanskaya St. 2, Sevastopol, Ukraine, 335000.

(Received December 3, 1993; revised September 29, 1994; accepted December 19, 1994.)